*Journal of Engineering Physics and Thermophysics, Vol. 75, No. 6, 2002*

# GAS FLOW IN A PLANE CHANNEL WITH OSCILLATING WALLS

**A. L. Tukmakov**

UDC 539.37:519.63

*Gas oscillations occurring in a plane channel in excitation of elastic walls which is symmetric relative to the longitudinal axis are investigated by the methods of numerical modeling. The spatial localization of transverse and longitudinal waves has been revealed and the character of resonance oscillations of the gas in the vicinity of the excitation region for different velocities of the flow has been established.*

Investigation of resonance oscillations of a gas in tubes and channels is associated with various technical applications [1]. For longitudinal oscillations of a gas resonant frequencies are determined by the formula $\omega_{mn} = n\pi c/(mL)$; prominence is given to the oscillations with frequencies of linear resonances at $m = 1$ and $n = 1, 2, 3, \ldots$, which is due to the occurrence of the highest-intensity discontinuous waves in their vicinity [1–3]. Nonlinear or subharmonic resonances occurring in excitation with frequencies $\omega_{mn}$, $m > 1$, are considered along with linear resonances. The longitudinal oscillations of a gas that are excited in a closed tube by a piston oscillating with frequencies of the first and second nonlinear resonances ($\omega_{21}$ and $\omega_{31}$) are investigated experimentally in [2], and the physical experiment of [2] is compared to a numerical one in [3].

In the present work, we investigate the motion of a gas in a plane channel. We consider the localization of transverse and longitudinal waves, assess the influence of the average velocity of the flow on the character of propagation of the waves in the gas, and reveal the features of oscillations related to the resonance properties of the channel in the transverse direction. We assume that the upper and lower channel walls are elastic for $-l \le x \le l$ and rigid beyond this interval and the channel cross section possesses a longitudinal axis of symmetry (Fig. 1a). The problem will be solved in a symmetric formulation: the calculation region will be bounded in the transverse direction by the longitudinal axis of symmetry and by the longitudinal channel wall (Fig. 1b).

To describe the gas motion in the channel we employ the system of Navier–Stokes equations for a compressible heat-conducting gas [4] written in a Cartesian coordinate system:

$$\mathbf{q}_t + \mathbf{F}_x + \mathbf{G}_y = 0\,, \tag{1}$$

where

$$\mathbf{q} = \begin{bmatrix} \rho \\ \rho u \\ \rho v \\ e \end{bmatrix};\quad \mathbf{F} = \begin{bmatrix} \rho u \\ \rho u^2 + p - \tau_{xx} \\ \rho uv - \tau_{xy} \\ (e + p - \tau_{xx})\, u - \tau_{xy} v + Q_x \end{bmatrix};\quad \mathbf{G} = \begin{bmatrix} \rho v \\ \rho uv - \tau_{xy} \\ \rho v^2 + p - \tau_{yy} \\ (e + p - \tau_{yy})\, v - \tau_{xy} u + Q_y \end{bmatrix};$$

$$Q_x = -k\frac{\partial T}{\partial x};\quad Q_y = -k\frac{\partial T}{\partial y};$$

$$\tau_{xx} = \mu\left(2\frac{\partial u}{\partial x} - \frac{2}{3}D\right);\quad \tau_{yy} = \mu\left(2\frac{\partial v}{\partial y} - \frac{2}{3}D\right);\quad \tau_{xy} = \mu\left(\frac{\partial u}{\partial y} + \frac{\partial v}{\partial x}\right);$$

Institute of Mechanics and Mechanical Engineering, Kazan Scientific Center, Russian Academy of Sciences, Kazan, Russia; email: tukmakov@mail.knc.ru. Translated from Inzhenerno-Fizicheskii Zhurnal, Vol. 75, No. 6, pp. 109–115, November–December, 2002. Original article submitted March 5, 2002.

1062-0125/02/7506-1379$27.00 

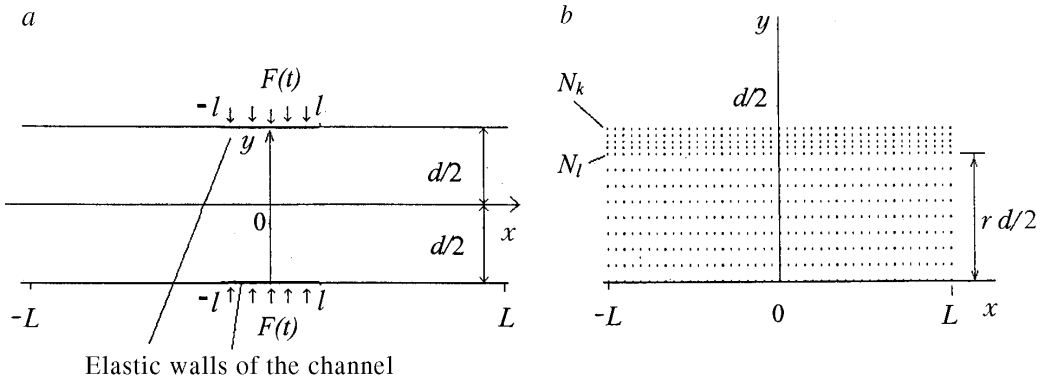


Fig. 1. Scheme of the channel (a) and fragment of the finite-difference grid (b).

$$D = \frac{\partial u}{\partial x} + \frac{\partial v}{\partial y}; \quad p = (\gamma - 1)\,(e - 0.5\rho\,(u^2 + v^2))\,.$$

System (1) in the region with variable boundaries is solved by introduction of the time-dependent generalized coordinates [4–6] $\xi = \xi(x, y, t)$, $\eta = \eta(x, y, t)$, $\tau = t$. In new variables, system (1) has the form

$$q_t^* + F_\xi^* + G_\eta^* = 0\,, \tag{2}$$

where

$$\mathbf{F}^* = \frac{1}{J}\begin{bmatrix} \xi_t\rho + \xi_x\rho u + \xi_y\rho v \\ \xi_t\rho u + \xi_x\,(\rho u^2 + p - \tau_{xx}) + \xi_y\,(\rho uv - \tau_{xy}) \\ \xi_t\rho v + \xi_x\,(\rho uv - \tau_{xy}) + \xi_y\,(\rho v^2 + p - \tau_{yy}) \\ \xi_t E + \xi_x\,((e + p - \tau_{xx})\,u - \tau_{xy}v + Q_x) + \xi_y\,((e + p - \tau_{yy})\,v - \tau_{xy}u + Q_y) \end{bmatrix};$$

$$\mathbf{G}^* = \frac{1}{J}\begin{bmatrix} \eta_t\rho + \eta_x\rho u + \eta_y\rho v \\ \eta_t\rho u + \eta_x\,(\rho u^2 + p - \tau_{xx}) + \eta_y\,(\rho uv - \tau_{xy}) \\ \eta_t\rho v + \eta_x\,(\rho uv - \tau_{xy}) + \eta_y\,(\rho v^2 + p - \tau_{yy}) \\ \eta_t E + \eta_x\,((e + p - \tau_{xx})\,u - \tau_{xy}v + Q_x) + \eta_y\,((e + p - \tau_{yy})\,v - \tau_{xy}u + Q_y) \end{bmatrix};$$

$$\mathbf{q}^* = \frac{1}{J}\begin{bmatrix} \rho \\ \rho u \\ \rho v \\ E \end{bmatrix}; \quad J = \begin{bmatrix} \xi_x & \xi_y & \xi_t \\ \eta_x & \eta_y & \eta_t \\ 0 & 0 & 1 \end{bmatrix}; \quad \xi_t = -x_t\xi_x - y_t\xi_y\,; \quad \eta_t = -x_t\eta_x - y_t\eta_y\,.$$

To solve it we used the McCormack explicit method of second order of accuracy with time splitting and a scheme of correction of fluxes [4, 6]. On a uniform grid, the McCormack scheme contains two steps implementing the transition to the next layer: the predictor step and the corrector step

$$\overset{\circ}{q}_{j,k} = q_{j,k}^n - \frac{\Delta t}{\Delta\xi}\,[F_{j+1,k}^n - F_{j,k}^n] - \frac{\Delta t}{\Delta\eta}\,[G_{j,k+1}^n - G_{j,k}^n]\,;$$

$$q_{j,k}^{n+1} = 0.5\,(q_{j,k}^n + \overset{\circ}{q}_{j,k}) - 0.5\,\frac{\Delta t}{\Delta\xi}\,[\overset{\circ}{F}_{j,k} - \overset{\circ}{F}_{j-1,k}] - 0.5\,\frac{\Delta t}{\Delta\eta}\,[\overset{\circ}{G}_{j,k} - \overset{\circ}{G}_{j,k-1}]\,.$$

Each spatial group **F** and **G** at the predictor and corrector steps is approximated by one-sided finite-difference operators. Thus, for example, the derivatives with respect to $\xi$ which enter into $F^n_{j+1,k}$ and $F^n_{j,k}$ are approximated by the left-hand difference schemes of first order of accuracy at the predictor step and by the right-hand ones at the corrector step while the derivatives with respect to $\eta$ are approximated by the central difference schemes of second order of accuracy. The derivatives with respect to $\eta$ which enter into $G^n_{j,k+1}$ and $G^n_{j,k}$ are approximated by the left-hand difference schemes of first order of accuracy while the derivatives with respect to $\xi$ are approximated by the central schemes. In calculations on a nonuniform grid with bunching near the lateral surface, we introduced the scheme of time splitting [4, 6]. On the finite-difference grid in the physical region ($x$, $y$) whose fragment is shown in Fig. 1b the step used for the $x$ axis is uniform. We prescribed $N_k$ nodes along the $y$ axis. The first $N_1$ nodes formed cells with a fixed step $\Delta y$ ($0 \le y \le rd/2$). Nodes with $N_1$ to $N_k$ ($rd/2 < y \le d/2$) formed cells with a finer step $\Delta y_1$. The parameter $r$ prescribed the boundary of the region with a small step. The region ($\xi$, $\eta$) was a unit square with uniform splitting along the axes.

The scheme of splitting for the region in question was prescribed by a symmetric sequence of one-dimensional operators. In the region bounded by the nodes with the subscripts $1 \le j \le N_j - 1$ and $2 \le k \le N_1$, the scheme had the form

$$q^{n+1}_{j,k} = P_\xi\left(\frac{\Delta t}{2}\right) P_\eta\left(\frac{\Delta t}{2}\right) P_\eta\left(\frac{\Delta t}{2}\right) P_\xi\left(\frac{\Delta t}{2}\right) q^n_{j,k}\,.$$

Each one-dimensional operator included the predictor and corrector steps. Thus, for example, the action of the operator $P_\xi(\Delta t/2)$ on the column vector $q^n_{j,k}$ which resulted in the transition to the intermediate value $\bar{q}_{j,k}$ lay in realization of two steps:

$$\overset{\circ}{q}_{j,k} = q^n_{j,k} - \frac{\Delta t}{\Delta\xi}\,[F^n_{j+1,k} - F^n_{j,k}],\quad \overline{q_{j,k}} = 0.5\,(q^n_{j,k} + \overset{\circ}{q}_{j,k}) - 0.5\,\frac{\Delta t}{2\Delta\xi}\,[\overset{\circ}{F}_{j,k} - \overset{\circ}{F}_{j-1,k}]\,.$$

In the region of bunching of the grid nodes $2 \le j \le N_j - 1$ and $N_1 \le k \le N_k - 1$, the splitting scheme involved $2n$ one-dimensional operators $P_\eta$:

$$q^{n+1}_{j,k} = P_\xi\left(\frac{\Delta t}{2}\right) P_\eta\left(\frac{\Delta t}{2n}\right) \ldots P_\eta\left(\frac{\Delta t}{2n}\right) P_\xi\left(\frac{\Delta t}{2}\right) q^n_{j,k}\,,$$

where $n = \Delta y/\Delta y_1$. The symmetric sequence of one-dimensional operators is required to preserve the second order of accuracy of the numerical method [4]. To suppress oscillations on shock waves we used the well-known Lax–Wendroff sound scheme of correction of fluxes described in [4] in detail.

The change in the shape of the elastic element caused the geometry of the calculation region to change. Rearrangement of the finite-difference grid in "physical" variables ($x$, $y$) and its mapping on a fixed finite-difference grid in "calculation" variables ($\xi$, $\eta$) were realized at each time step. The rearrangement parameters $\xi_x$, $\xi_y$, $\eta_x$, $\eta_y$, $x_t$, $y_t$, $\xi_t$, and $\eta_t$ involved in representation of the system of the equations of motion of the gas in generalized moving coordinates [4, 5] were determined and transition to the next time layer was implemented according to the McCormack scheme.

On solid surfaces, we set the adhesion conditions for the components of the gas velocity — on the plate surface, they were set equal to the corresponding components of the plate velocity. We set homogeneous boundary conditions of the second kind for the density, energy, and temperature at all the boundaries of the calculation region, including the plate surface. We determined the temperature, density, and velocity of the gas at the internal nodes of the calculation region at the initial instant of time. On the axis of symmetry, we set $u(j, 1) = u(j, 2)$ and $v(j, 1) = -v(j, 2)$ for the velocity components at the nodes of the finite-difference grid (Fig. 1b).

To describe the motion of elastic wall portions we used the system of dynamic geometrically nonlinear equations of the theory of thin plates that obey the Kirchhoff–Love hypothesis [7]:

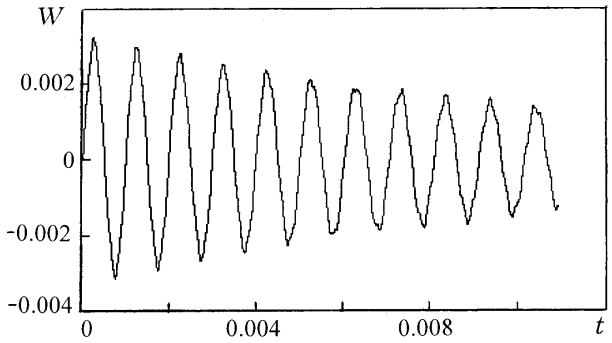


Fig. 2. Oscillations of the midpoint of the plate. *W*, m; *t*, sec.

$$\frac{\partial^2 V}{\partial t^2} = \frac{E}{\rho_{\text{pan}}(1-\nu^2)}\frac{\partial^2 V}{\partial x^2} + \frac{E}{\rho_{\text{pan}}(1-\nu^2)}\frac{\partial W}{\partial x}\frac{\partial^2 W}{\partial x^2} + \frac{Z_\tau}{\rho_{\text{pan}}};$$

$$\frac{\partial^2 W}{\partial t^2} = -\frac{D}{\rho_{\text{pan}}}\frac{\partial^4 W}{\partial x^4} - \alpha\frac{\partial W}{\partial t} + \frac{Eh}{\rho_{\text{pan}}(1-\nu^2)}\left(\frac{\partial V}{\partial x} + \frac{1}{2}\left(\frac{\partial W}{\partial x}\right)^2\right)\frac{\partial^2 W}{\partial x^2} + \frac{Z_{\text{n}}}{\rho_{\text{pan}}}. \quad (3)$$

For the longitudinal edges of the plate (Fig. 1a) we specified the conditions of rigid sealing:

$$W = 0, \quad V = 0, \quad \partial W/\partial x = 0 \quad \text{for} \quad x = \pm l. \quad (4)$$

It was assumed that the plate is fixed at the initial instant of time:

$$W = 0, \quad V = 0, \quad \partial W/\partial t = 0, \quad \partial V/\partial t = 0 \quad \text{for} \quad t = 0, \quad -l \le x \le l. \quad (5)$$

The tangential component of the load is equal to zero while the normal component contains the rigid and slave parts. The slave character of the load is determined by the excess pressure on the surface of the elastic plate. The external pulse excitation $F(t)$ is a rigid component independent of the shape of the oscillating surface:

$$Z_{\text{n}} = F(t) + p_0 - p, \quad Z_\tau = 0, \quad F(t) = F_0 t \quad \text{for} \quad t < T_{\text{r}}, \quad F(t) = 0 \quad \text{for} \quad t \ge T_{\text{r}}. \quad (6)$$

System (3) with conditions (4)–(6) was solved by the finite-difference method with the use of implicit difference schemes of second order of accuracy [8]. In analyzing the solution of the system, we constructed the power spectra of the oscillations of the gas pressure at different points of the channel and the power spectra of deflection oscillations at different points of the plate:

$$S_k = \left| \frac{1}{\sqrt{n}} \sum_{j=1}^{n} X_j \exp\left(-i\frac{2\pi kj}{n}\right) \right|^2,$$

where $X_j$ is the value of the signal at the instant of time $t_j = j\Delta t$, $S_k$ is the frequency-dependent discrete component of the power spectrum, $\Delta t$ is the time step, and $i$ is the imaginary unit. The gasdynamic part of the software system was tested by comparing the results of numerical modeling and the existing experimental data [3]. The method used to model the dynamics of the elastic element has been investigated in [9].

The numerical experiment lay in loading elastic channel walls by a single triangular pressure pulse, which resulted in the oscillations of the plates constituting portions of the upper and lower walls for $-l \le x \le l$. The pulse duration was equal to half the period of natural oscillations of the plates at the lower resonant frequency. We considered gas flows caused by the oscillations of the elastic channel walls for different velocities of the middle flow.

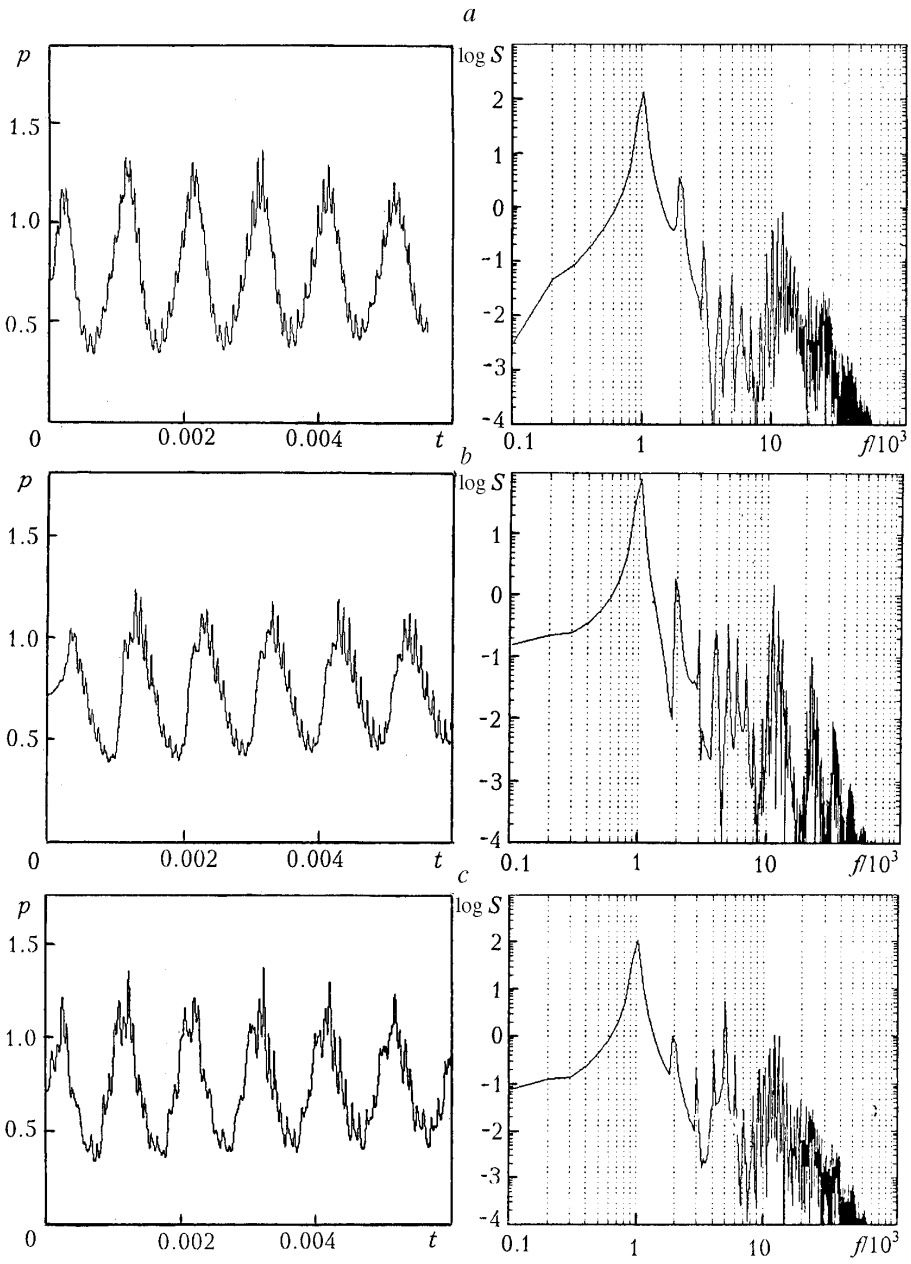


Fig. 3. Time dependences of the pressure and their power spectra: 1) on the channel axis at the point ($x$ = 0.06, $y$ = 0); b) on the surface of the oscillating wall ($x$ = 0.06 m); c) on the channel axis at the point ($x$ = 0.2 m, $y$ = 0). The pressure is assigned to the pressure of an undisturbed gas at $t$ = 0. $f$, Hz.

The channel length was selected in such a manner that the disturbances on the time interval under study failed to reach the inlet and outlet boundaries. The calculations for the channel of height $d$ = 0.03 m were carried out for the following parameters of the plate: $h$ = 0.002 m, $2l$ = 0.2 m, $E = 10^{11}$ N/m$^2$, $\nu$ = 0.3, and density $\rho_{pan}$ = 4500 kg/m$^3$. In solving the elastic problem, the number of nodes of the finite-difference grid was $N$ = 60. We took air with $\gamma$ = 1.4, $R$ = 278 J/(kg·K), $T_0$ = 290 K, and $\rho_0$ = 1.2 kg/m$^3$ as the gas filling the channel. The results were obtained on the computational grid with parameters $N_j$ = 297, $N_k$ = 25, $N_1$ = 9, and $r$ = 0.8, where $N_1$ is the number of the nodes for $y \le rd$. In calculating, the time step was $\Delta t = 3 \cdot 10^{-8}$ sec. In the figures presented below, the pressure and the velocity components are assigned to the pressure and the velocity of sound of an undisturbed gas.

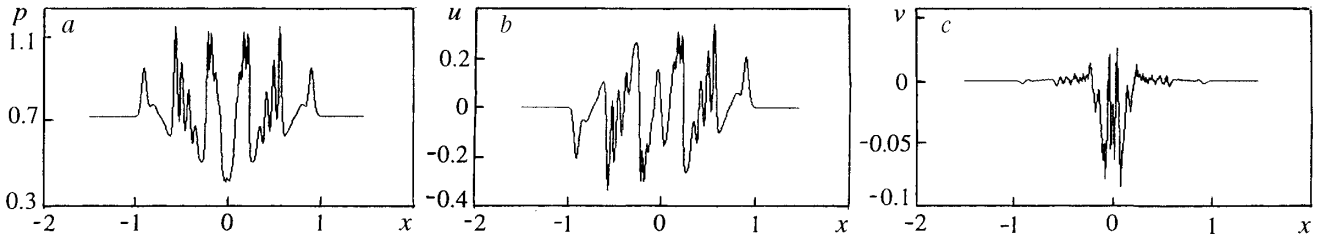


Fig. 4. Distributions of the pressure and of the longitudinal and transverse components of the velocity of the gas at the instant of time $t$ = 0.0025 sec in the absence of middle flow. The pressure and the velocity are assigned to the pressure and the velocity of sound in an undisturbed gas at $t$ = 0.

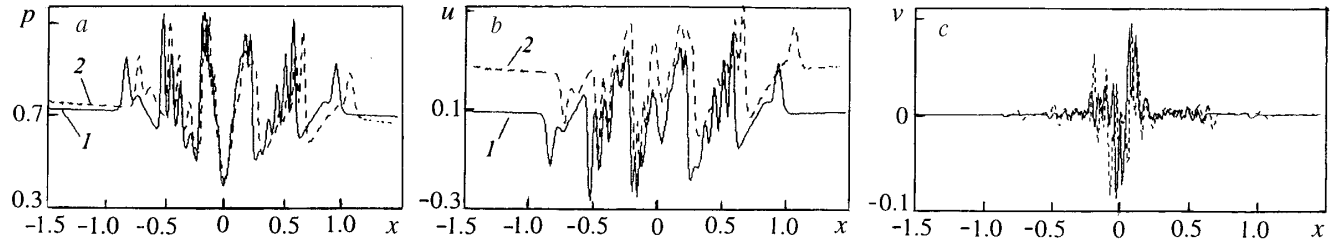


Fig. 5. Distributions of the pressure and of the longitudinal and transverse velocity components at the instant of time $t$ = 0.0025 sec for different velocities of the middle flow: 1) velocity of the flow is $0.1c_0$; 2) velocity of the flow is $0.3c_0$. The pressure and the velocity in the figures are assigned to the pressure and the velocity of sound in an undisturbed gas at $t$ = 0.

*1. Oscillations of the Gas in the Channel in the Absence of Middle Flow.* The deflection of the midpoint of the plate as a function of time is given in Fig. 2. The frequency of oscillations occurring upon external unloading is $f \approx 1000$ Hz; the oscillation mode is symmetric. The oscillations of the plates cause the oscillations of the gas column concentrated between the channel walls. The portion of the channel adjacent to the plates ($-l \le x \le l$, $-d/2 \le y \le d/2$) (Fig. 1a) can be considered as an acoustic resonator whose eigenfrequencies are determined by the channel height. The $Q$ factor of such a resonator depends on the dissipative loss and loss by the formation of shock waves and by radiation along the channel. Because of the symmetric character of excitation, the peak values of the pressure are observed both near the oscillating wall and on the longitudinal axis of symmetry. For a channel height of $d$ = 0.03 m and a velocity of sound of $c$ ($T$ = 290 K) = $(\gamma RT)^{1/2}$ = 336 m/sec the frequency of the first linear acoustic resonance of the gas column in the transverse direction is $f_{1,1} = c/2d$ = 5600 Hz [1–3, 10, 11] and it will be observed near the walls at one fixed plate and one oscillating plate. Since the peak values of the pressure on the axis of symmetry are produced by converging waves that traversed half the channel height, this frequency is doubled and is $f_{1,1}$ = 11,200 Hz. The ratio of frequencies $f_{1,1}/f \approx 11$, which leads to the generation of the subharmonic acoustic resonance $f_{1,11}$ manifesting itself in the frequency modulation of the carrier acoustic signal of frequency $f$ by oscillations with a frequency $f_{1,1}$ [2, 3]. Figure 3a gives the pressure as a function of time and the corresponding power spectrum of oscillations on the channel axis ($x$ = 0.06 m, $y$ = 0), and Fig. 3b gives the same characteristics on the surface of the oscillating wall for $x$ = 0.6 m. The power spectra of pressure oscillations contain frequencies which are multiples of the frequency of oscillations of the elastic walls. The resonance $f_{1,11}$ is pronounced both on the axis of symmetry and at the surface of the oscillating plate (Fig. 3a and b). Transverse-type oscillations (along the $y$ axis) occurring with a frequency $f_{1,1}$ are discontinuous in character and are presented by waves with a steep leading front and a mildly sloping trailing front. With distance from the resonator boundaries ($x = \pm l$), we observe a decrease in the power of the oscillations occurring with a frequency $f_{1,1}$ along the longitudinal axis (Fig. 3c).

The distribution of the pressure and of the transverse velocity component $v$ possess symmetry relative to the axis $x$ = 0 (Fig. 4a and b). The longitudinal component of the velocity $u$ on the channel axis is a function of odd symmetry relative to the point $x$ = 0 (Fig. 4b). It should be noted that whereas the waves of pressure and longitudinal

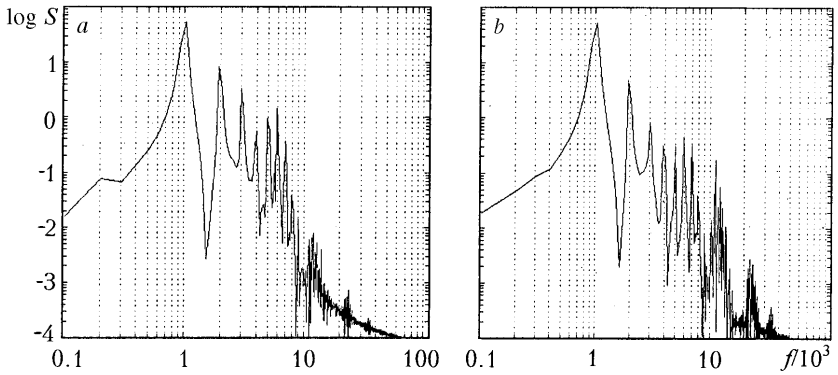


Fig. 6. Power spectra of pressure oscillations on the channel axis for a velocity of the gas flow of $0.1c_0$ at the points which are located upstream and downstream relative to the oscillating plate: a) $x = -0.2$ m; b) $x = 0.2$ m.

velocity are propagating along the channel, the transverse oscillations remain localized near the plate. The amplitudes of oscillations of the transverse velocity are substantially smaller outside this region than inside it (Fig. 4c). The distribution of the transverse component along the longitudinal axis is alternating in character, which indicates the vortices propagating along the channel axis. Vortices with the highest rotational velocity are adjacent to the plate on the left and on the right and have opposing directions of rotation, which is demonstrated by the identical direction of the transverse velocity components (Fig. 4c).

With distance from the region ($-l \le x \le l$, $-d/2 \le y \le d/2$) the transverse oscillations are transformed to longitudinal ones: the amplitude of the transverse oscillations decreases more rapidly than the amplitude of the longitudinal ones. In the case of the transverse oscillations of the gas, subharmonic resonances spatially localized in the vicinity of the oscillating plate are generated, whereas the longitudinal oscillations are observed throughout the channel.

2. *Influence of Middle Flow on Gas Oscillations in the Channel.* If oscillations of the gas in the channel occur for a nonzero middle flow, the distribution of the pressure and velocity fields loses its symmetry. The difference of the velocities of downstream and upstream propagation of a disturbance wave leads to the fact that the lengths of the waves running streamwise and against the stream become dissimilar (Fig. 5a and b). The difference in the wavelengths on both sides of the oscillation resource increases with the velocity of the flow. At the same time, the distribution of the transverse-velocity field remains concentrated near the oscillating plate (Fig. 5c). Unlike the oscillation mode for a zero middle flow, the vortices adjacent to the plate acquire the identical direction of rotation: the transverse velocity component has different signs on both sides of the midpoint of the plate ($x = 0$). The time interval between pressure pulses at points which are symmetric relative to $x = 0$ makes it possible to determine the flow velocity. A comparison of the power spectra of pressure oscillations at the points on the axis of symmetry of the channel shows that high-frequency oscillations of the gas that manifest themselves in subharmonic resonance remain localized in the vicinity of the oscillating plate. Figure 6 gives the power spectra of pressure oscillations at the points $x = \pm 0.2$ m on the channel axis for a flow velocity of $0.1c_0$. The character of the power spectra enables us to state that with distance upstream from the disturbance source the high-frequency components of the spectra decay more rapidly than in the direction of middle flow.

Thus, the results of the calculation of the gas dynamics in the channel carried out in the case of local excitation of the walls demonstrate that the region adjacent to the oscillating plates possesses resonance properties for transverse oscillations. When the frequency of oscillations of the plates coincides with the frequency of subharmonic resonance of the gas column in the transverse direction, we observe modulation of the carrier acoustic signal by the oscillations with a frequency of the first linear resonance for the cross section of the channel. With distance from the region adjacent to the oscillating plates, transformation of the transverse oscillations to longitudinal oscillations occurs: the amplitude of the transverse oscillations decreases more rapidly than the amplitude of the longitudinal ones. A comparison of the power spectra of pressure oscillations enables us to state that with distance upstream from the disturbance source the high-frequency spectrum components decay more rapidly than in the direction of middle flow.

This work was carried out with support from the "Integration" Federal Targeted Program, the Foundation for Research and Development of the Republic of Tatarstan, and the Russian Foundation for Basic Research.

## NOTATION

$x$ and $y$, longitudinal and transverse coordinates in the physical region; $\xi$, $\eta$, generalized coordinates corresponding to them; $u$ and $v$, longitudinal and transverse components of the gas velocity; $t$, time; $\rho$, $p$, $T$, and $e$, density, pressure, temperature, and total energy of the gas; $\mu$, molecular viscosity; $\gamma$, adiabatic exponent; $k$, thermal conductivity; $Q_x$ and $Q_y$, heat fluxes; $\tau_{xx}$, $\tau_{xy}$, and $\tau_{yy}$, shear stresses in the gas; $c$, velocity of sound in the gas; $\overset{\circ}{q}_{j,k}$, $\overset{\circ}{F}_{j,h}$, and $\overset{\circ}{G}_{j,k}$, values of the components of the vectors **q**, **F**, and **G** upon realization of the predictor step; $f_{n,m} = nc/(m \cdot 2d)$ ($m$, $n$ = 1, 2, 3, ...), resonant frequencies of the gas column in the transverse direction; $f$, oscillation frequency of the elastic plate; $2L$, channel length; $d$, channel height; $Z_\tau$ and $Z_n$, tangential and normal components of the dynamic load; $W$ and $V$, deflection and tangential movement of fixed (Lagrangian) points of the middle surface; $h$ and $\rho_{pan}$, thickness and density of the panel material; $E$, elastic modulus; $\nu$, Poisson coefficient; $R$, universal gas constant; $S$, oscillation-power spectrum; $2l$, length of the elastic plate; $\alpha$, coefficient of structural damping; $T_r$ and $F_0$, rise time and intensity of the external-load pulse; $j$ and $k$, indices (subscripts) of the nodes of the finite-difference grid in the gas in the direction of the $x$ and $y$ axes; $N_j$ and $N_k$, corresponding numbers of nodes of the finite-difference grid; $r$ and $N$, numerical coefficient and number of nodes in the transverse direction that prescribe the boundaries of the wall region with a fine grid. Subscripts: n, normal; pan, panel; 0, value of the parameters at the initial instant of time; r, rise.

## REFERENCES


1. M. A. Ilgamov, R. G. Zaripov, R. R. Galiullin, and V. B. Repin, *Appl. Mech. Rev.*, **49**, No. 3, 137–154 (1996).
2. R. G. Zaripov, R. I. Davydov, and N. V. Sonin, *Prikl. Mekh. Tekh. Fiz.*, **40**, No. 6, 61–63 (1999).
3. A. L. Tukmakov and R. G. Zaripov, *Izv. Vyssh. Uchebn. Zaved., Aviats. Tekh.*, No. 1, 64–67 (2001).
4. C. A. J. Fletcher, *Computational Techniques for Fluid Dynamics 1. Fundamental and General Techniques* [Russian translation], Moscow (1991).
5. J. L. Steger, *AIAA J.*, **16**, No. 7, 679–686 (1978).
6. V. M. Kovenya, G. A. Tarnavskii, and S. G. Chernyi, *Use of the Method of Splitting in Problems of Aerodynamics* [in Russian], Novosibirsk (1990).
7. A. S. Vol'mir, *Flexible Plates and Shells* [in Russian], Moscow (1956).
8. A. S. Vol'mir, *Shells in Liquid and Gas Flows. Problems of Aeroelasticity* [in Russian], Moscow (1976).
9. A. L. Tukmakov, *Prikl. Mekh. Tekh. Fiz.*, **41**, No. 1, 183–188 (2000).
10. A. L. Tukmakov, *Inzh.-Fiz. Zh.*, **74**, No. 5, 39–43 (2001).
11. A. L. Tukmakov, *Teplofiz. Aéromekh.*, **8**, No. 1, 101–108 (2001).